Heliyon 9 (2023) e18434

Contents lists available at ScienceDirect

Heliyon

journal homepage: www.cell.com/heliyon

Solar irradiance estimation and optimum power region localization in PV energy systems under partial shaded condition

Ambe Harrison [a,*], Njimboh Henry Alombah [b], Jean de Dieu Nguimfack Ndongmo [c]

[a] Department of Electrical and Electronics Engineering, College of Technology (COT), University of Buea, P.O.Box Buea 63, Cameroon
[b] Department of Electrical and Electronics Engineering, College of Technology, University of Bamenda, P.O. Box 39, Bambili, Cameroon
[c] Department of Electrical and Power Engineering, Higher Technical Teacher Training College (HTTTC), University of Bamenda P.O. Box 39 Bambili, Cameroon

ARTICLE INFO

Keywords:
PV
Partial shading conditions
Irradiance estimator
Optimal power region
MPPT

ABSTRACT

The efficient operation of PV systems relies heavily on maximum power point tracking (MPPT). Additionally, such systems demonstrate complex behavior under partial shading conditions (PSC), with the presence of multiple maximum power points (MPP). Among the existing MPPT algorithms, the conventional perturb and observe, and incremental conductance stand out for their high simplicity. However, they are specialized in single MPP problems. Thus, due to the existence of multiple MPPs under PSC, they fail to track the global MPP. Compared with the conventional schemes, the modified conventional algorithms, and several existing MPPT variants introduce a trade-off between complexity and performance. To enhance the simplicity of the PV system, it is crucial to adapt the operation of the simple conventional algorithm to scenarios under PSC. To achieve such an adaptation, the power-voltage curve that conventionally admits multiple MPPs under PSC must be converted to an equivalent curve having only a single MPP. To address such a requirement, this paper introduces a novel approach to the fast determination of the MPP. A consistent methodology for reducing the complex multiple MPP problem of PV systems under PSC, to a single MPP objective, is put forward. Thus such reduction enhances the tracking environment for simple conventional MPPT algorithms under partial shading. Studies of the PV array behavior for 735 partial shading patterns revealed an interesting possibility of reducing the classical PV curve to 8.2620% of its actual area. The newly established area is an optimum power region that accommodates a single MPP. To arrive at such a reduction, an intelligent neural network-based predictor, incorporating a cost-effective and reliable solar irradiance estimator is put forward. Unlike existing methods, the approach is free from the direct and expensive measurement of solar irradiance. The predictor relies on the PV array current and voltage only to precisely determine the optimum power region of the PV system.

1. Introduction

Increasing energy demands and growing environmental concerns have sparked a great deal of interest in nonconventional energy sources, such as solar. The use of photovoltaic (PV) cells allows the easy conversion of solar energy into electrical energy. The materialization of PV sources presents several key benefits including low maintenance cost, green energy conversion, and little or no

* Corresponding author.
E-mail address: ambe.harrison@ubuea.cm (A. Harrison).

https://doi.org/10.1016/j.heliyon.2023.e18434
Received 28 March 2023; Received in revised form 11 July 2023; Accepted 17 July 2023
Available online 20 July 2023

presence of rotating components. Despite these benefits, the high initial cost of energy production remains a crucial impediment to their effective application [1]. Thus maximizing their operating efficiency stand out as a viable option for moderating their cost. Additionally, the operation of PV systems features some level of nonlinearity, which makes it difficult to track their maximum power point (MPP). Furthermore, the variations in environmental irradiance and temperature cause more fluctuations in the MPP. Faced with such continuous variation, it is crucial to continuously track the MPP. Consequently, a series of maximum power point tracking (MPPT) algorithms have been reported in different scientific literature MPP [2–6]. As revealed by the literature, the classical conventional algorithm such as perturb and observe (P&O), and incremental conductance algorithm (INC) stand out as the simplest and most popular approaches. Under partial shading scenarios (non-uniform irradiance), the power-voltage (PV) curve of the PV system contains several MPPs. The global maximum power point (GMPP) is the MPP with the highest power, while the local maximum power point (LMPP) is the MPP with the lowest power. Classically, the conventional MPPT algorithm cannot distinguish between the LMPPs and the unique GMPP consequently, they get stuck at the former. Thus, partial shading is a crucial issue for PV systems as it can result in a tremendous loss of power. The results of the findings conducted in Ref. [7] revealed a drop of efficiency by up to 99.98% recorded during different critical partial shading scenarios. Thus partial shading conditions (PSC) is an undesired phenomenon in the operation of PV systems. Its adverse effect can lead to the long-term deterioration of the PV module performance [8]. Over the last few years, numerous researchers have focused important attention on the efficiency concerns of PV systems under PSC. Global maximum power point tracking (GMPPT) is one of the most important outcomes of recent research outcomes.

To surmount the challenges of the PV systems under partial shading conditions [9], combined a variable step-size P&O, and an inspection algorithm to track the GMPP. The method features a good performance with a noticeable increase in PV systems efficiency as compared with the conventional MPPT algorithm. However, slow tracking convergence and oscillations around the GMPP are the main shortcomings of the latter work. To effectively tackle the shortcomings of the conventional MPPT algorithms with PSC, several modified schemes have been established [10–12]. Most of these modified conventional algorithms introduce a trade-off between complexity and performance. The modified INC presented in Ref. [10] can track the GMPPT under extreme environmental conditions as well as under load variation scenarios. However, the slow tracking process is the main shortcoming of the approach, which comes from the sequential comparison of the power at different peaks in order to effectively track the GMPP. To effectively track the GMPP, special consideration must be integrated regarding the power-voltage (P–V) search space area of the PV system. The moderate performance of several GMPPT algorithms is a potential consequence of large search space. Under such consideration, a reduction of the GMPPT algorithm's search space is expected to leverage the PV system's performance. In light of search space reduction [13], confined the tracking region to 10% of the initial P–V curve. Furthermore, the work shows that there is a consistent improvement in the P&O algorithm's performance. Although the latter approach is an important opening toward effective search space reduction, it does not provide a structured methodology for precisely determining the limits of this search space. Furthermore, the study is limited to PV systems operating under uniform irradiance conditions.

In a systematic review [14], showed that intelligent optimization algorithms, especially the nature-inspired swarm search mechanisms play a major role in MPPT, especially for PV systems under PSC [15]. on the other hand, proposed a swarm-inspired algorithm based on hybrid particle swam optimization (PSO) and Fireworks algorithm (FWA). The combined approach targets the problem of balancing between exploration and explosion sparks operators, which is effectively addressed by the PSO velocity operator and the FWA mutation and explosion sparks operator. The method achieves significantly better efficiency and tracking speed as compared to the singular PSO and FWA. Also inspired by nature-based optimization solutions [16], proposes a two-stage MPPT controller using a combined artificial bee colony (ABC) and simultaneous heat transfer search (SHTS) algorithm. The hybrid ABC-SHTS algorithm targets effective balancing between exploration and exploitation in search for the global maximum power point and archives better performance MPPT performance than numerous other optimization-based algorithms.

As revealed by the literature it is evident that optimization algorithms are successful in tracking the MPP under PSC. Their strong affinity for the GMPP specializes them in PV systems under PSC. However, they only provide moderate performance with regard to tracking speed, which limits the overall PV system's efficiency. Furthermore, faced with a large search space, they present a slow response with respect to the tracking process. Moreover, the complexity of such algorithms makes them not feasible for practical implementation. Therefore, search space reduction represents a fruitful direction for improving the performance of such algorithms.

In this work, by incorporating optimal power region identification and global reduced search space, we aim to establish a simple yet powerful approach to leveraging the performance of PV systems under PSC. We investigate the behavior of the PV system under diverse partial shading patterns and consistently establish that it is possible to reduce the complex multiple MPP problem of the PV array under the partial shading scenario, to a single MPP objective, with significantly reduced search space. As a consequence, the overall system gains a significant reduction of the tracking search space. Additionally, the GMPP is precisely identified within such a reduced search region, thus ensuring a favorable tracking environment for the simple conventional MPPT algorithms. The key advantage of this approach lies in the fact that the simple conventional MPPT algorithm can be effectively integrated within the PV system for tracking the GMPP under partial shading scenarios without facing problems of local convergence at the local MPP. Thus this work completely leverages the complexity of the PV system under non-uniform irradiance conditions. The remainder of this paper is structured as follows: A detailed modeling of the PV system is provided in section 2. A systematic methodology for estimating the solar irradiance on PV modules under partial shading is put forward in section 3. In section 4, a consistent methodology for localizing optimal power regions in PV systems under partial shading is presented. In section 5, the result and discussion of this paper's findings are consistently illustrated. Furthermore, the relevance of this study is highlighted in section 6. Finally, this paper is concluded in section 7.

2. PV modelling and characterization under PSC

2.1. Single diode model

The existing works of literature report several techniques for modeling solar panels [17]. The single-diode model has been consistently adopted for several PV studies due to its simplicity and satisfactory accuracy [17].

As seen in Fig. 1, the model is constituted around a Photocurrent source, responding to solar irradiance (G) through the flow of electric current I_{ph}. Additionally, the model features a nonlinear component, semiconductor-diode D, with current I_D. Parasitic resistances R_p, R_s makes the model more practical. Thus they carry the currents I_p and I_{pv} respectively. The mathematic model relating the PV current I_{pv} and voltage V_{pv} is presented as:

$$I_{pv} = I_{ph} - I_s\left[exp\left(\frac{q\left(V_{pv} + N_s I R_s\right)}{N_s nkT}\right) - 1\right] - \frac{V_{pv} + I_{pv}R_s}{R_p} \tag{1}$$

Thus from the above relation, the parameters q, n, k, T, I_s, and N_s represent the charge constant, diode ideality factor, Boltzmann constant, cell operating temperature, diode saturation current, and the number of series-connected cells. From the same equation, the parameters I_{ph}, and I_s depend heavily on environmental conditions. Thus, it is obvious to write I_{ph} as $I_{ph}(G,T)$ and I_s as $I_s(T)$ to capture the sense of reliance on environmental G and T. These parameters can be formulated mathematically as illustrated in Eqs. (2) and (3):

$$I_{ph}(G,T) = \frac{G}{G_{ref}}\left(I_{ph-ref} + K_i\left(T - T_{ref}\right)\right) \tag{2}$$

$$I_s(T) = I_{s-ref}\left(\frac{T}{T_{ref}}\right)^3 exp\left[\frac{qE_g}{nk}\left(\frac{1}{T_{ref}} - \frac{1}{T}\right)\right] \tag{3}$$

More so, the shunt resistance depends on the cell irradiance, and can be written as follows:

$$R_p = R_{p,-ref}\left(\frac{G}{G_{ref}}\right) \tag{4}$$

The terms R_{p-ref}, and G_{ref} in Eq. (4) denote the reference values of the parallel and shunt resistance and irradiance respectively.

2.2. Description of PV system considering partial shading

A PV array is an assembly of parallel or/and series-connected solar panels [10]. As a consequence, the electrical power produced by the array is an arithmetic combination of respective power produced from the individual modules. In the series connected configuration, non-uniform irradiance results in different output power on solar modules. Under this condition, the shaded module is constrained to operate in reverse bias mode, hence behaving as a load instead of a PV source [10]. This results in power dissipation and induces hotspots or self-heating that can irreversibly deteriorate the shaded module. In order to mitigate such a problem, Bypass diodes as seen in Fig. 2 (b), are introduced in the array to avoid hotspots during shading scenarios. However, the protection offered by these diodes introduces complexity in the current-voltage (I–V) and P–V characteristics of the PV module, as they lead to the generation of multiple peak power points. On the other hand, under uniform irradiance as seen in Fig. 2(a), the blocking diodes are reversed bias and have no impact on the PV array. Moreover, as seen in Fig. 2, Blocking diodes are often connected in series with the PV array line to prevent the backflow of the current into the PV.

Considering the simple configuration in Fig. 2, made of three modules in the string. The first array as seen in Fig. 2(a) is under uniform irradiance conditions (UIC) while the second array in Fig. 2(b) is under PSC. Under PSC, the first two modules in Fig. 2(b) are subjected to a solar irradiance of 1000 W/m^2, while the last module on the string receives 500 W/m^2. By so doing, we subject the array under non-uniform irradiance. Ideally, for series connected array, the array voltage, $V_{pv-array}$ is the sum of the module voltages (V_{pv}), such that the electric current flowing through them is ideally the same.

It is illustrated in Fig. 3, that the I–V and P–V of the PV array under UIC demonstrate the presence of a single maximum power point. This point occurs at (181.3V, 51.48W) MPP-UIC. Conversely, under the specified PSC, the operation of the array reveals a local

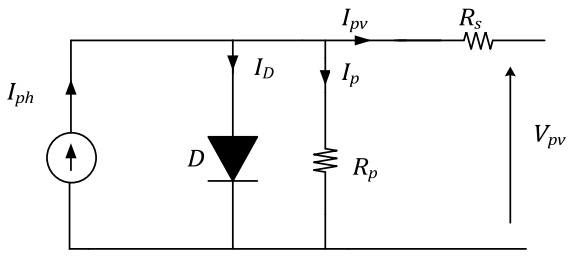

Fig. 1. Single diode model of the PV.

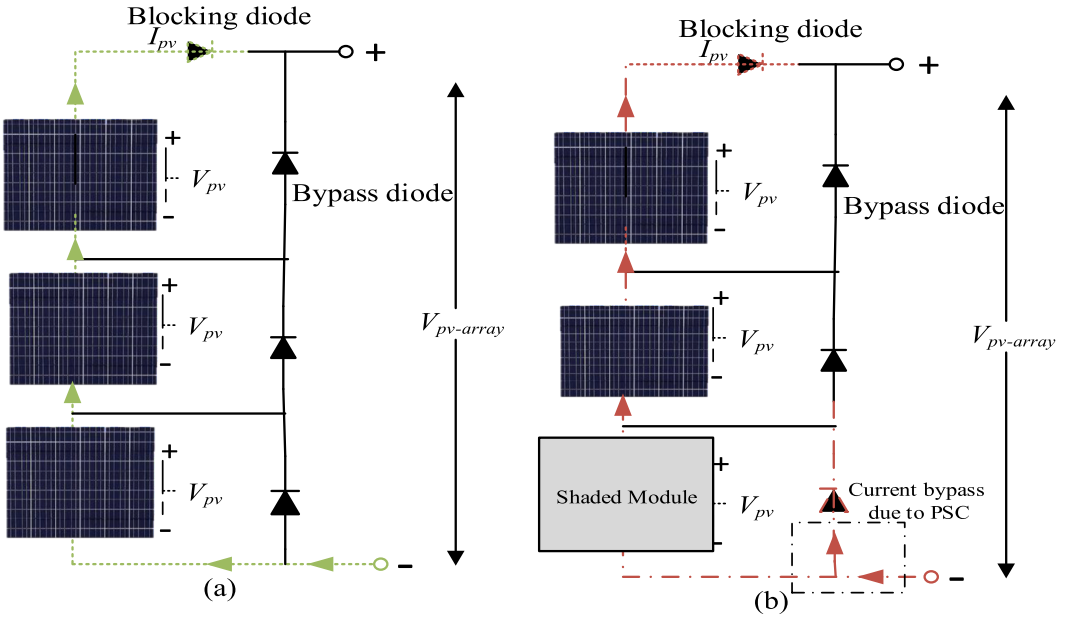

Fig. 2. Operation of the PV array (a) under uniform irradiance condition (b) under partial shading condition.

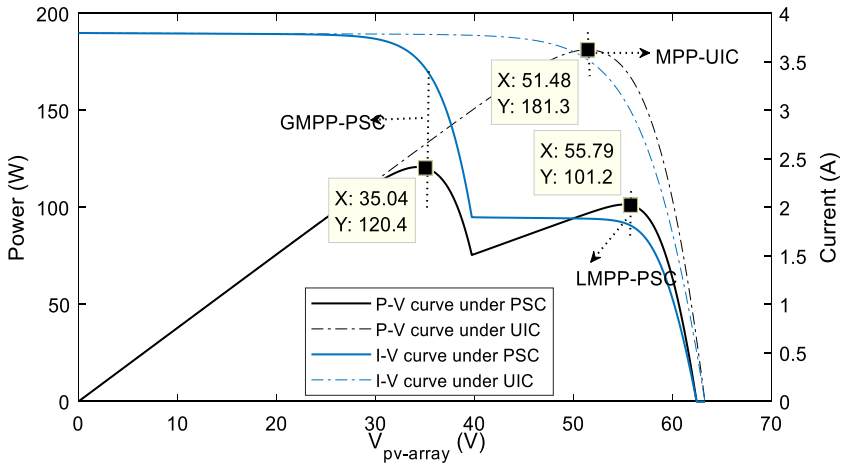

Fig. 3. Characteristics of the PV array under UIC and PSC (Descriptive example).

maximum power point (LMPP-PSC) and a global maximum power point (GMPP-PSC). It is further seen in Fig. 3, that the array power at the (GMPP-PSC) is greater than that at the (LMPP-PSC). Furthermore, it is evident that the maximum power available from the array under UIC (181.3W) is greater than the global maximum power under PSC. Thus this clearly shows the adverse power deterioration effect of partial shading on the PV system. Faced with such a scenario, it becomes imperative to ensure that the PV array operates at the GMPP-PSC. Generally, patterns of PSC are not fixed, making it very difficult to precisely identify the position of the GMPP-PSC. This suggests that proper identification of the GMPP region under PSC can enhance the maximum power tracking potential of simple conventional MPPT algorithms. Numerous GMPPT algorithms often fail to track the GMPP because of improper identification of the regions containing the GMPP, this is the case with all the conventional MPPT algorithms in the literature.

In this paper, we propose to accurately locate the optimal regions in the PV array. The optimal power region contains a single maximum power point. To carry out this study we are going to resort to estimating the solar irradiance of partially shaded modules.

All the investigations in this paper are based on the solar module with specifications illustrated in Table 1. It is worth noting that the complete model of this solar panel is fully available and implemented in MATLAB/Simulink. The three main parameters of the model that is $[n, R_s\ R_p]$ are [1.6, 0.2039, 993.9] as specified in the table. The module can be combined to form an array of any specific size. In this paper, we reconsider an array, made of solar panels connected in a series configuration

Table 1
Characteristics of the PV module.

Parameter	Value
Maximum power voltage (V_{mpp})	17.14V
Maximum power current (I_{mpp})	3.5248A
Voltage at open circuit (V_{oc})	21.1V
Current at short circuit (I_{scc})	3.8V
Temperature coefficient of V_{oc} (A_v)	− 80mV/°C
Maximum power (P_{max})	60.4281 W
Temperature coefficient of I_{scc} (K_i)	0.065%/°C
Number of series cells (N_s) [$n, R_s\ R_p$]	36 [1.6, 0.2039, 993.9]

3. Solar irradiance estimation under PSC

Solar irradiance measurement and estimation have always been an issue of concern in the context of PV systems research. In numerous PV studies, the measurement or good estimate of solar irradiance is indispensable. A series of techniques have been proposed in existing literature to estimate solar irradiance. These techniques vary according to the PV context and application. In generalized applications, solar irradiance can be measured directly using a Pyranometer instrument. The Pyranometer is very expensive and therefore not a cost-effective approach to getting informed on solar irradiance. The method presented in Ref. [18] exploits the short-circuit current of the solar panel to indirectly compute the solar irradiance. This approach is cost-effective and simple but can only provide moderate accuracy. The method presented in Ref. [19] exploits the environmental dynamics of the equivalent circuit of the PV module to compute the solar irradiance. The accuracy of the method is conditioned by the PV operation at the maximum power point. As a consequence, if the PV is not effectively operating at the MPP the approach will fail to estimate the solar irradiance. Moreover, the method is limited to PV systems under uniform irradiance conditions. A similar method in Ref. [20] estimates the solar irradiance and module temperature for PV systems under single maximum power point operations. The work in Ref. [21] presents a very accurate estimator of solar irradiance. The strength of the latter estimator lies in the fact that it requires only the PV voltage and current sensors to provide an estimate of the irradiance with guaranteed stability. Though the work is exceptional in performance, it is not applied to PV systems under partial shading scenarios.

To the best of our knowledge, the estimation of the solar irradiance under PSC, especially in the context of maximum power point tracking has not received attention. All the papers that we came across are limited to solar irradiance estimation under UIC. Information related to the irradiance on individual modules could serve as a guide to locating the global maximum power point in PV conversion systems. Thus in this study, we synthesize a simple estimator of solar irradiance for solar panels under partial shading scenarios.

The proposed estimator exploits the array of electric current and output voltage to indirectly compute solar irradiance on the respective modules. The synoptic diagram of the estimator is presented in Fig. 4. Therefore, exploiting the nonlinear behavior of the PV

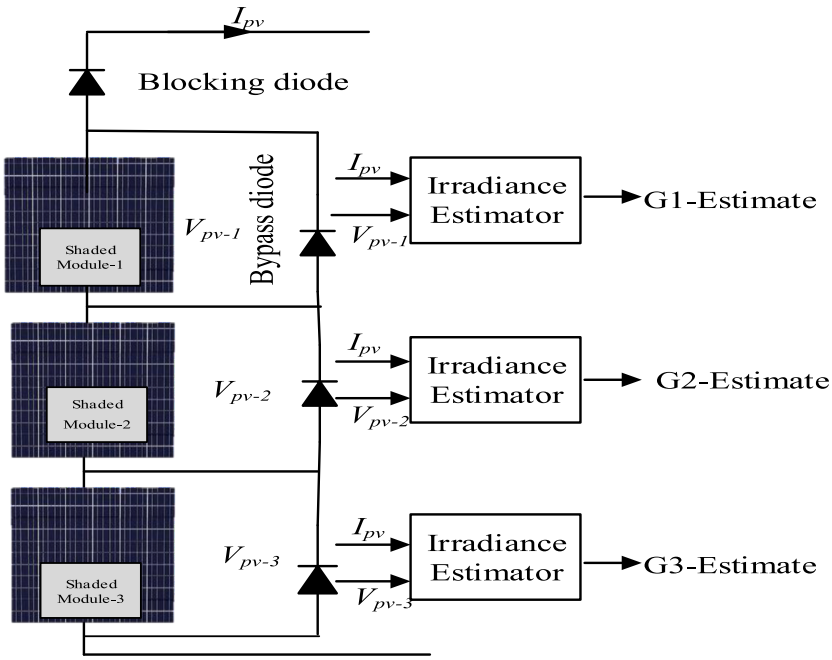

Fig. 4. Solar irradiance Estimator under PSC.

module, one can reparametrize the nonlinear equation presented in Eq. (1) to seek the estimate of the actual irradiance to which the shaded modules respond.

We are going to design the irradiance estimator for one PV module and generalize it for any number of modules under PSC. By combining Eq. (1) and Eq. (5) with a simple rearrangement we have:

$$I_{pv} = I_{ph}(G,T) - I_s\left[exp\left(\frac{q\left(V_{pv}+N_sIR_s\right)}{N_snkT}\right)-1\right] - \frac{G_{ref}\left(V_{pv}+I_{pv}R_s\right)}{GR_{p-ref}} \tag{5}$$

Further simplification of Eq. (5) results in Eq. (6):

$$I_{pv} = I_{ph}(G,T) + F\left(I_{pv},V_{pv},T\right) - \frac{\mathrm{A}_0}{G}\left(V_{pv}+A_1I_{pv}\right) \tag{6}$$

Where $A_o = \frac{G_{ref}}{R_{p-ref}}$, $A_1 = R_s$, and $F(I_{pv},V_{pv},T)$ defined as:

$$F\left(I_{pv},V_{pv},T\right) = -I_s\left[exp\left(\frac{q\left(V_{pv}+N_sIR_s\right)}{N_snkT}\right)-1\right] \tag{7}$$

To design the estimator, we reparametrize the current-voltage characteristics such that it exhibits a monotonic behavior. With measurements of the PV current $I_{pv}(t)$, voltage $V_{pv}(t)$, and operating temperature $T(t)$. On any shaded module, a measurable signal based on Eq. (7) can be introduced as illustrated in Eq. (8):

$$y(t) = I_{pv}(t) - F\left(I_{pv}(t),V_{pv}(t),T(t)\right) \tag{8}$$

The signal $y(t)$ can adopt the following nonlinear structure:

$$y(t) = \Omega(G,t) \tag{9}$$

Where, $\Omega(G,t)$ is obtained as:

$$\Omega(G,t) = I_{ph}(G,T) - \frac{\mathrm{A}_0}{G}\left(V_{pv}+A_1I_{pv}\right) \tag{10}$$

Given that $V_{pv}(t), I_{pv}(t),$ and $T(t)$ are readily available for measurements, we can recall the Immersion and Invariance (I&I) synthesis [21–23], to design the estimator law as

$$\dot{\widehat{G}} = k[y - \Omega(\widehat{G})], k > 0 \tag{11}$$

Where, $\widehat{G}$ is the estimate of the actual irradiance and k is the parameter of the estimator.

As proved in Appendix. A, the function $\Omega(G,t)$ exhibit a strict monotonous behavior, which warrants that $\lim_{t\to\infty}\widehat{G}(t) = G$, hence the estimate of the irradiance $\widehat{G}$ converges to the actual irradiance. Furthermore, the Lyapunov proof shows that the system is asymptotically stable (see Appendix. A).

$$\dot{\widehat{G}} = k\left[I_{pv}(t) - F\left(I_{pv}(t),V_{pv}(t),T(t)\right) - I_{ph}(G,T) - \left(A_1V_{pv}+A_2I_{pv}\right)\right] \tag{12}$$

Generally, the irradiance estimator law for the respective PV module under PSC can be written as in Eq. (12). The constant k is a design parameter, which affects the dynamic response of the estimator, hence has to be properly designed according to specific dynamic objectives.

As illustrated by Eq. (12) the proposed estimator of solar irradiance requires just the measurement of current I_{pv} and voltage V_{pv}. In conformity to Ref. [24] the high-precision hybrid voltage-current INA160 sensor which measures up to 15A cost less than 10$. Conversely, the deployment of solar irradiance meters (Pyranometer) is an accurate but very expensive alternative. According to Ref. [25], the popular silicon cells Pyranometer cost in the range of 200-500. Although comparatively less expensive than other classes of Pyranometers, they present weak sensitivity to all wavelengths. They are only sensitive within 350 nm to 1100 nm of wavelength, which results in spectral errors for changing and unsteady solar spectrum [25]

Alternatively, first and second-class Pyranometers have the advantages of high sensitivity and minimum spectral error but at a higher cost. According to Ref. [25], their price varies between 500$ and 2,100$. It is therefore evident than the proposed estimator of solar irradiance is a more cost-effective strategy for getting informed on solar irradiance.

4. Localization of the optimal power region

The accurate localization of optimal power regions requires a broad study of the array under diverse patterns of partial shading conditions (PSC). In this paper, we consider an array made up of a single string of three series-connected solar panels. The characteristics of the PV module is illustrated in Table 1. Furthermore, we consider 735 different patterns of solar irradiance (G_1, G_2, G_3) for the three PV modules as seen in Fig. 5. For every pattern of PSC, we computed and extracted the optimal parameters data that is the GMPP power and voltage.

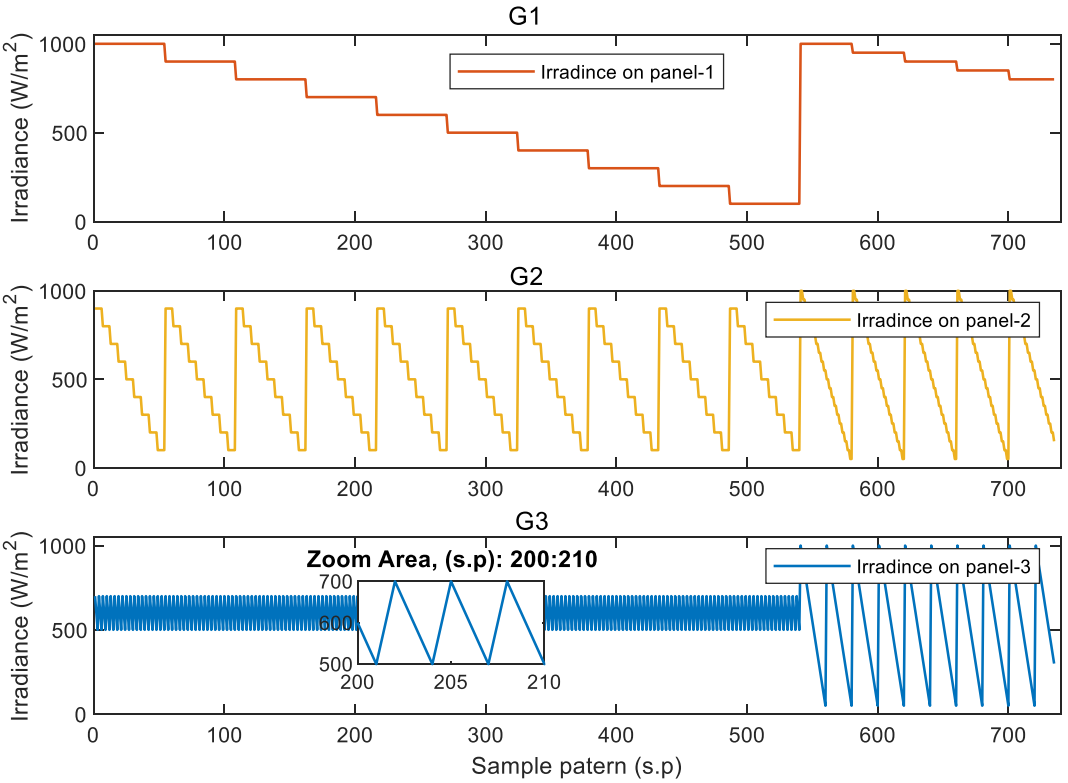

Fig. 5. 735 different patterns of PSC for three PV modules.

The GMPP for the 735 PSC patterns is presented in Fig. 6. About 550 GMPP appear in the same positions. It can be seen that the GMPPT can be confined between three optimal regions, namely regions 1,2, and 3. Hence each optimal region can be considered to have a minimum and maximum optimal voltage level. This implies that there exist three optimal minimum voltage levels and three optimal maximum voltage levels as seen in Table 2. The minimum and maximum voltage level in optimal region 1 was found to be 16.67V and 17.14V respectively. The voltage levels for region 2 and region 3 can be seen in Table 2.

Using the information in Table .2, an optimal voltage predictor can be constructed. Therefore, we train an ANN with a dataset made of 400 PSC patterns. The ANN receives as inputs, the estimate of solar irradiance from the three PV modules under PSC and outputs a minimum and maximum voltage level according to Table 2. The ANN was trained using a Bayesian Regularization training algorithm for better generalization, with a simple setting of one hidden layer and 10 neurons. As illustrated in Fig. 7 the training process smoothly converges after the 999th iteration with the best mean square error found to be 0.11469, which is quite small for a PV array. Therefore, with the irradiance estimator and the ANN power network, we can build an optimal power region predictor. The proposed predictor system is illustrated in Fig. 8. It consists of a PV array under PSC, estimators for each PV module, and an ANN model for predicting the

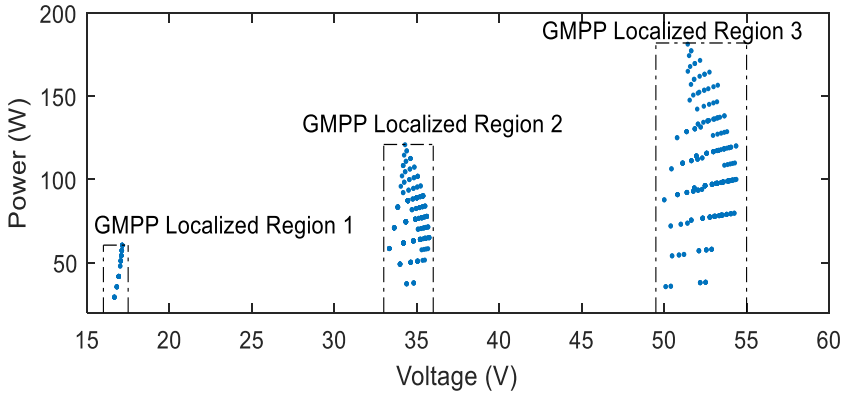

Fig. 6. Distribution of the GMPP for 735 PSC patterns.

Table 2
Optimal power areas.

Optimal regions	$V_{min}(V)$	$V_{max}(V)$
Region 1	16.67	17.14
Region 2	33.34	35.68
Region 3	50.11	54.37

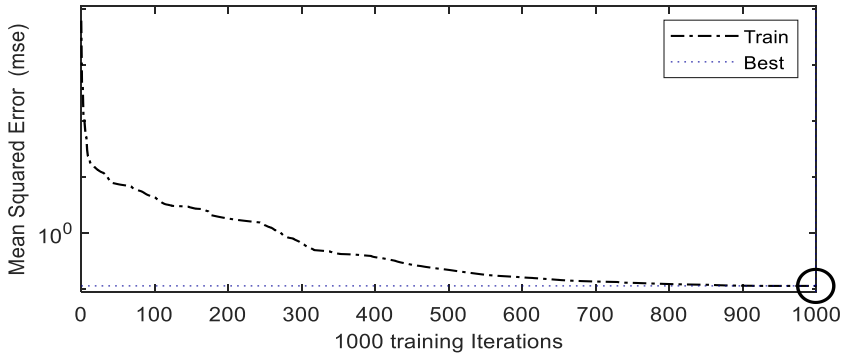

Fig. 7. Convergence of the mean square error during the training process.

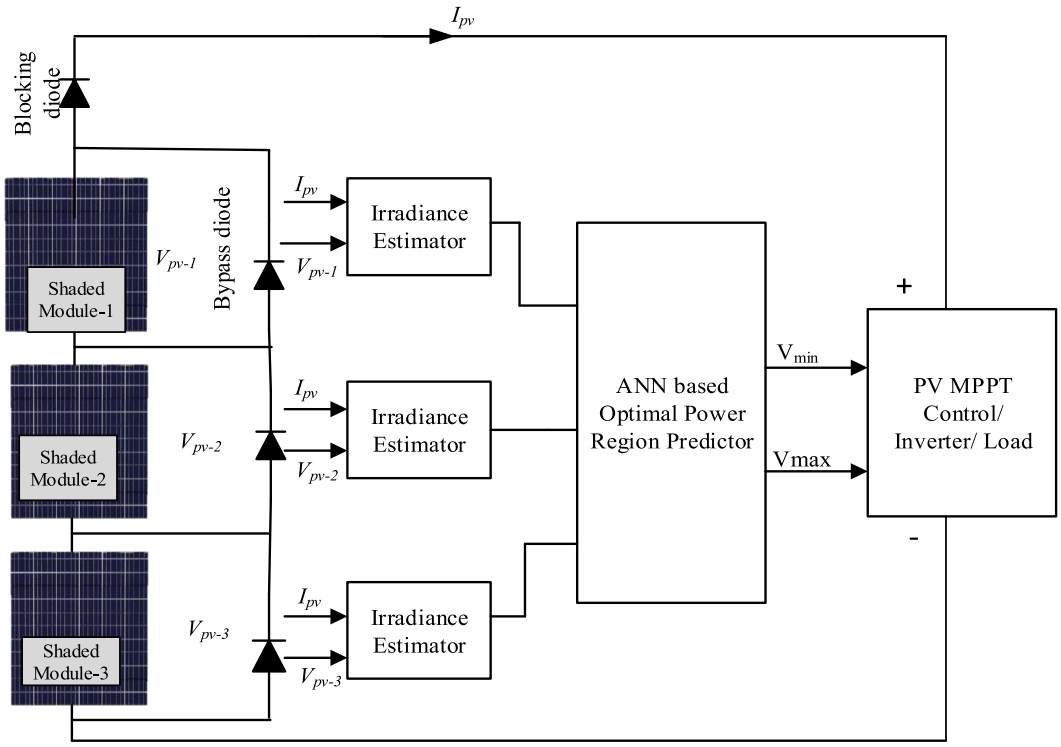

Fig. 8. Synoptic structure of the proposed system.

lower and upper bounds of the optimal power region. Each estimator receives two inputs, that is, the voltage across the specific solar panel and the array current.

5. Main results and discussions

Several experiments were performed in MATLAB/Simulink to assess the proposed optimal power localization scheme. The MATLAB/Simulink design for the overall system is presented in Fig. 9. PSC investigations are often carried out with temperatures held

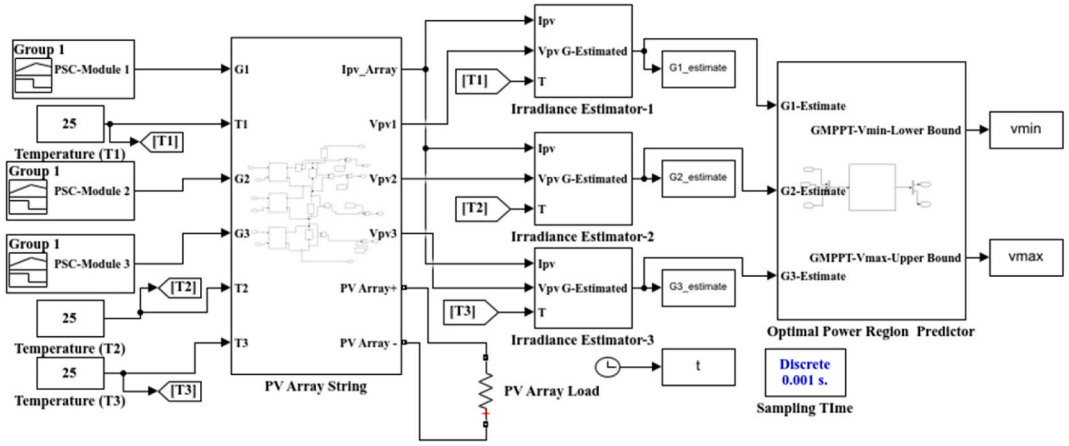

Fig. 9. Implementation of the proposed system in Simulink/MATLAB.

constant [10]. In our experiments, the temperature was fixed at 25 $^{\circ}C$ for all the modules as seen in Fig. 9. Furthermore, a resistive load of value 100Ω and a data sampling time of 0.001s, was considered for all the experiments.

To proceed with the investigations, we choose the suitable value of the estimator design parameter (k) which offered a satisfactory response. To carry out this experiment, the three modules were exposed to uniform irradiance (1000 W/m^2) and coupled with their estimators. The dynamic response of the estimator for varying values of k is presented in Fig. 10. It can be confirmed that the settling time of the estimator reduces with the magnitude of k. By so doing the estimator can be designed with a settling time goal. In this work, we desire a settling time (t_s) objective of 40 ms. Therefore, the parameter of the estimator (k) was fined tuned till the goal was attained. It can be seen in Fig. 10 that the objective was obtained at the value of $k = 50000$. Therefore, this value of k was adopted for all investigations under PSC. To further our investigations under PSC, we adopted three main patterns as presented in Table 3. The patterns were chosen to cover all the possible forms of appearance of the GMPP. According to Ref. [10], GMPP can appear in three possible ways; at the extreme right of the curve, the extreme left of the PV curve, and between two local maxima.

In the first experiment, the array was exposed to PSC governed by Pattern-B as shown in Table 3. It can be seen in Fig. 11 that three estimators rapidly converge and track the actual solar irradiance with zero steady-state error. The estimator of the solar panel 1 converges to 400 W/m^2. Estimator 2 converge to the actual solar irradiance of 1000 W/m, while estimator three converged to 600 W/m^2. Furthermore, is evident that the proposed system identified the optimal power area as region-3. The lower voltage bound of the predictor converged to 50.11V, while the upper voltage bound converged to 54.37V. These two voltage levels conform with the voltage level for the said region as presented in Table 2. This is further justified by the fact that the optimal power point (GMPP) falls within these two voltage levels as seen in Fig. 12. Hence the optimal voltage region for the PV array under PSC-B was accurately localized. The

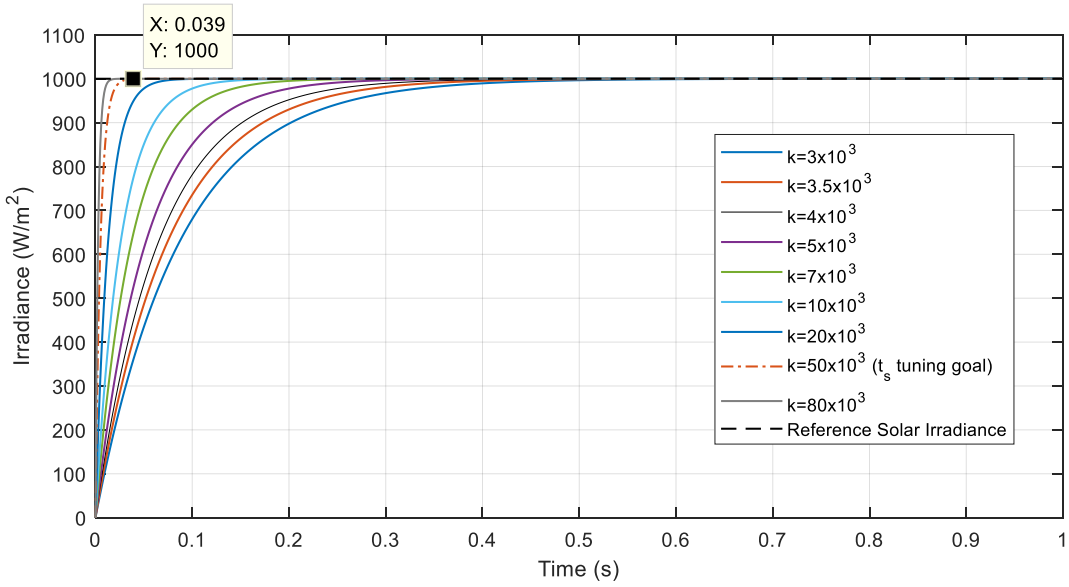

Fig. 10. Dynamic response of the estimator for different values of the estimator design parameter (k).

Table 3
PSC pattern used to assess the proposed system.

No	G1	G2	G3	New Area of the P–V curve
B	400	900	600	9.9%
C	500	300	600	5.36%
D	200	100	700	1.627%

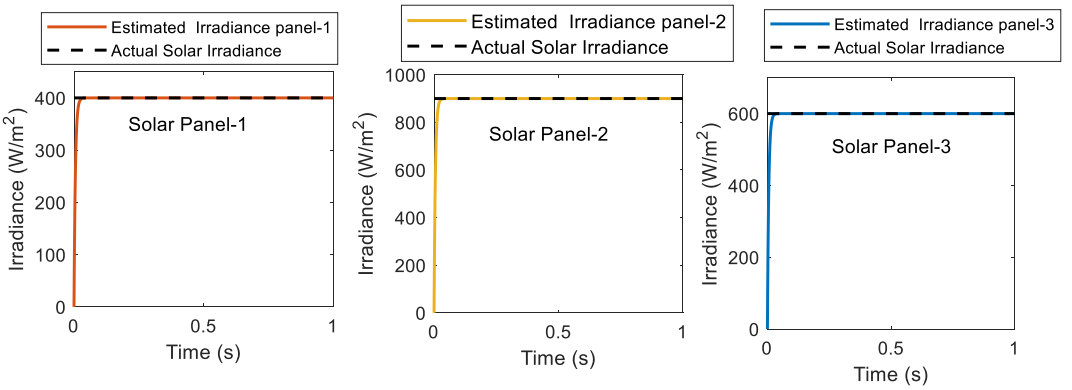

Fig. 11. Response of the estimator under PSC- B

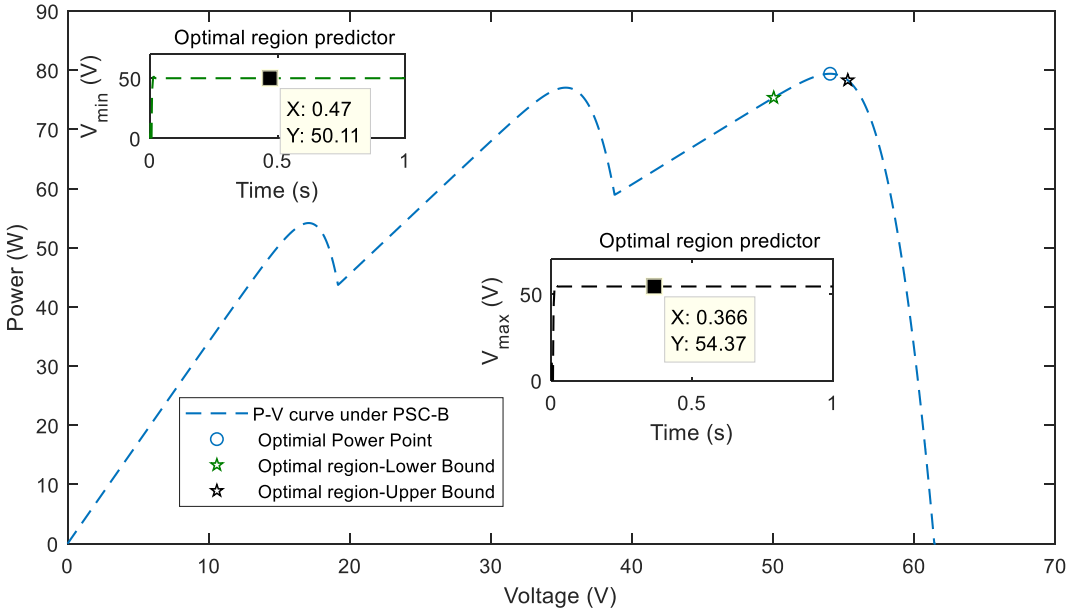

Fig. 12. Localization of the optimal power region under PSC-B

localized area is quite small. Its main importance lies in the fact that; it is void of any local maxima. Hence by applying the proposed localization scheme, the multiple power point problems can be reduced to a single power point problem which suggests that a conventional single maximum power point tracking algorithm could be deployed within this area to fast-track the optimal power point (GMPP). The new area of the P–V curve running from the lower bound to the upper bound of the optimal region was found to cover just 9.9% of the actual P–V curve.

During the second experiment, the array was subjected to PSC-C. Under this shading condition, as seen in Fig. 14, the GMPPT appears between two local maxima. It is noteworthy appreciating the noticeable response of the three estimators as seen in Fig. 13. The estimators rapidly converged to the actual values of actual solar irradiance under the partially shaded modules. Also, it is illustrated that the proposed system identified the optimal power area belonging to region-2. The lower voltage bound of the predictor rapidly converged to 33.34V, while the upper voltage bound converged to 35.68V. These two voltage levels conform with the voltage level for

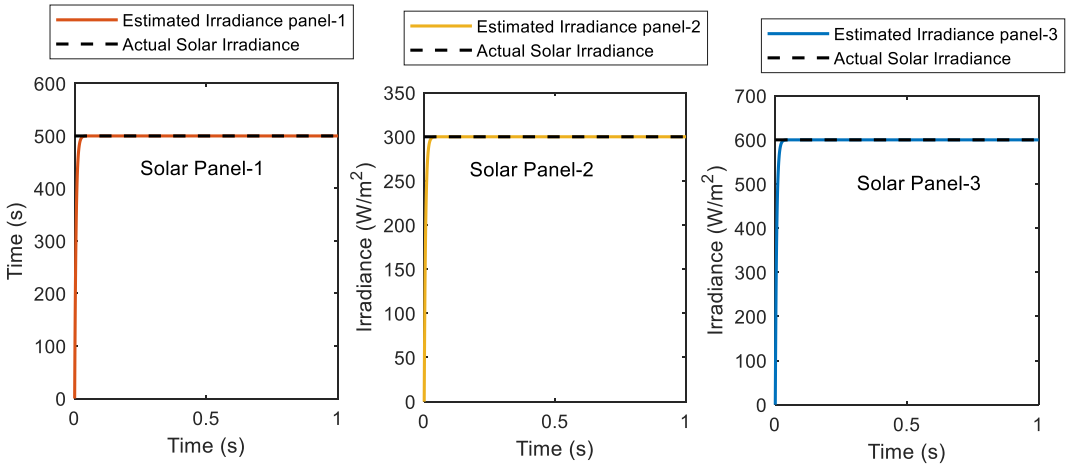

Fig. 13. Response of the estimator under PSC- C

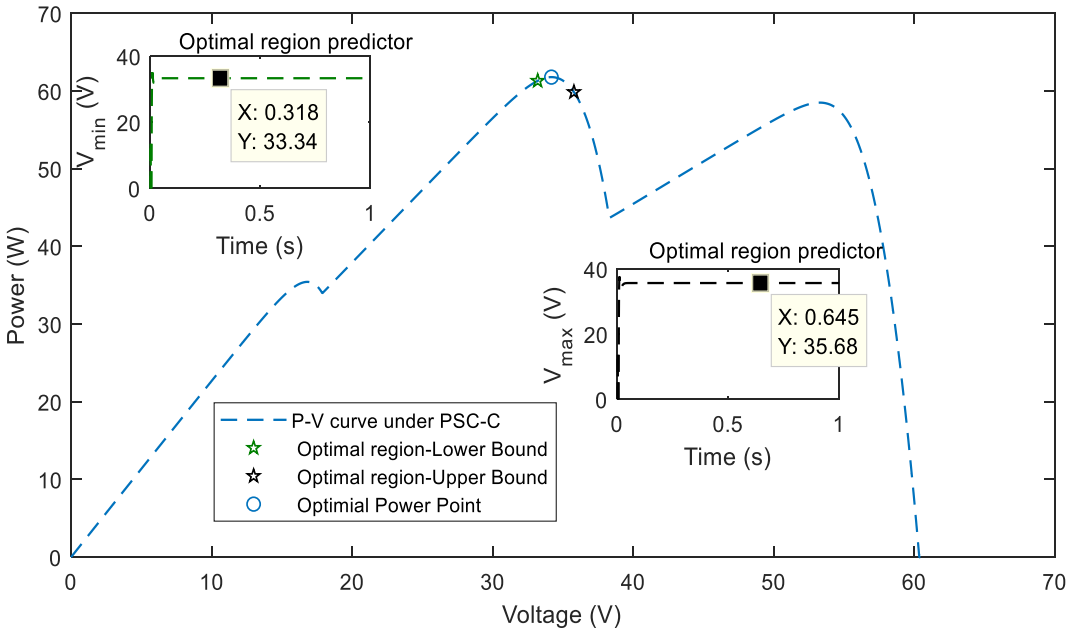

Fig. 14. Localization of the optimal power region under PSC-C

the said region as presented in Table 2. This is supported by the fact that the optimal power point (GMPP) falls within these two voltage levels as seen in Fig. 14. Hence the optimal voltage region for the PV array under PSC-C was accurately localized. The new area of the P–V curve running from the lower bound to the upper bound of the optimal region was found to cover just 5.36% of the actual P–V curve, which is small. It can be confirmed by inspection that the said areas are lower than the area under PSC-B.

In the third experiment, the PV array was subjected to PSC-D. Under this shading condition, as seen in Fig. 16 the GMPPT appears at the extreme left of the local maxima. The good dynamic response of the estimators as revealed by Fig. 15 can be exalted as they rapidly converge to the actual value of the solar irradiance. Estimator-1, which was coupled with PV module 1 converged to the expected irradiance of 200 W/m^2. The estimator in PV module 2 converged to the expected irradiance value of 100 W/m^2. While the estimator related to the third PV panel converged to the desired 700 W/m^2. One can confirm that all the estimators satisfied the settling time objective of (40 ms). This suggests the good robustness of the estimators.

It can be further seen in Fig. 16 that the proposed system identified the optimal power area to belong to region-1. The lower voltage bound of the predictor rapidly converged to 16.67V, while the upper voltage bound converged to 17.14V. These two voltage levels conform with the voltage level for the said region as presented in Table 2. This is supported by the fact that the optimal power point (GMPP) falls within these two voltage levels as seen in Fig. 16. Hence the optimal voltage region for the PV array under PSC-D was accurately localized. The new area of the P–V curve running from the lower bound to the upper bound of the optimal region was found

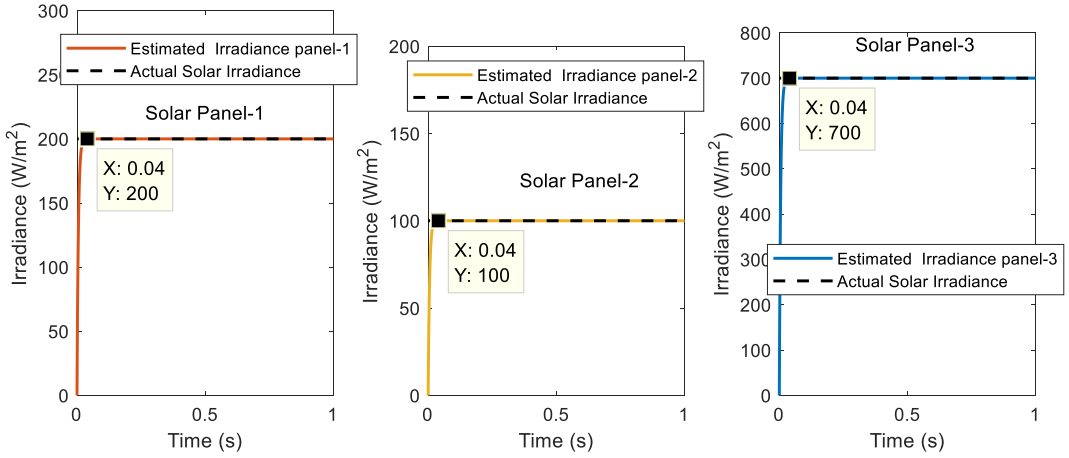

Fig. 15. Response of the estimator under PSC- D.

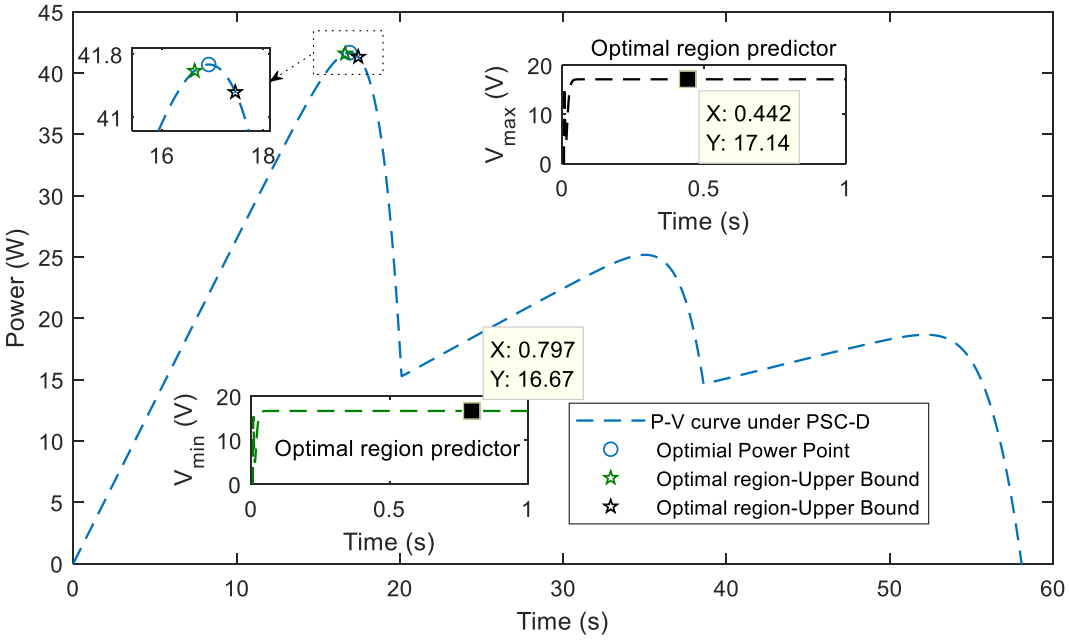

Fig. 16. Localization of the optimal power region under PSC-D.

to cover just 1.627% of the actual P–V curve, which is the smallest among the three PSC conditions. This very small area suggests that the estimator almost tracks the optimal power point.

The above investigations assumed that the partial shading profile under the PV array is constant. In practice, the array could be subjected to variations in partial shading patterns. Hence a fourth experiment was performed, which involves the assessment of the proposed system under varying PSC patterns. The variations constitute the systematic change of patterns from PSC-B to PSC-C and finally to PSC-D. These variations were introduced at the time instants of 0.3s and 0.6s respectively.

The estimation response of the estimator under varying PSC patterns is presented in Fig. 17, while the dynamic voltage response of the different optimal voltage predictors for the different PV panels is illustrated in Fig. 18. It can be seen that they all rapidly converge to the actual value of irradiance on the different partially shaded modules. This further confirms the good robustness of the estimator even under changing environmental conditions. Furthermore, the dynamic response of the optimal voltage level is presented in Fig. 18. It can be seen that when the array was under PSC-B during the time range of 0 to 0.3s, the lower voltage bound of the optimal power region was found to be 50.11V, while the optimal voltage bound was recorded to be 54.37V, which is in exact conformity with the expected voltage level for region 3 as shown in Table .2. At the time 0.3s when the PSC pattern was rapidly changed to PSC-C, we observed a small transient phenomenon (overshoot) in the response of the voltage level. However, the convergence of the voltage to the desired level was satisfactory. A similar condition can be observed for the change of pattern from PSC B to PSC-D. A small transient

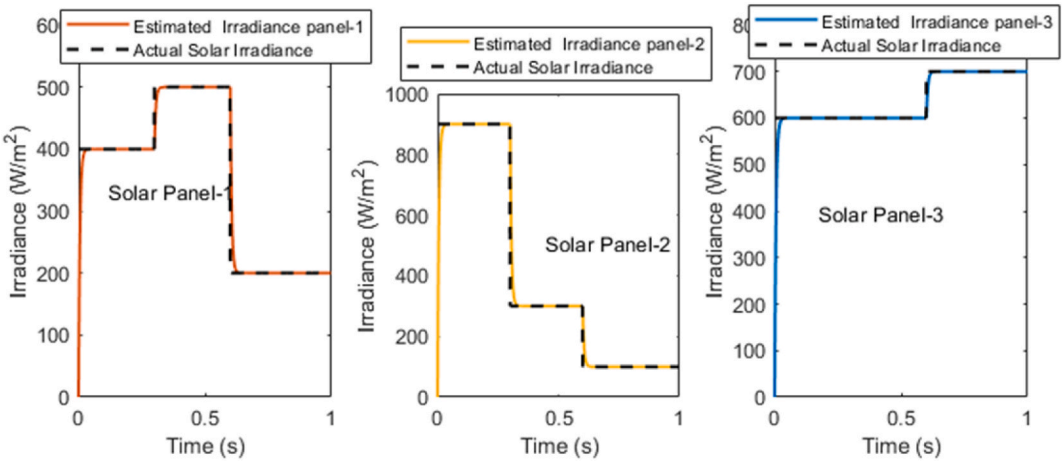

Fig. 17. Response of the Estimator under changing PSC patterns.

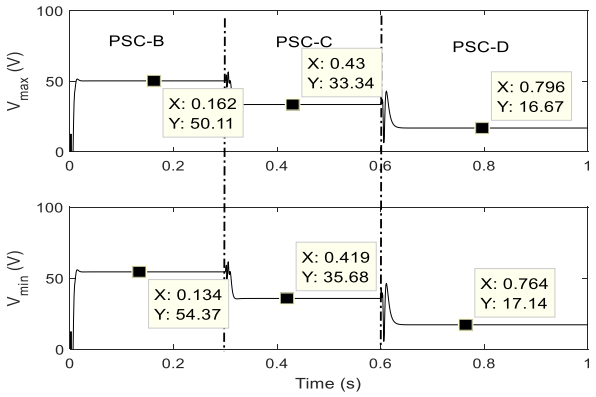

Fig. 18. Dynamic response of the lower and upper voltage bound for the optimal power regions.

phenomenon was observed then the lower and upper voltage levels converged to 16.67V, and 17.14V respectively, which conforms to the expected voltage level in optimal region 1. Finally, to validate the proposed optimal power region localization scheme, the system was subjected to 700 partial shading conditions and the newly established area of the P–V curve set by the lower and upper voltage levels was computed. The distribution of the area of the new P–V curve is presented in Fig. 19.

As seen in Fig. 19, the maximum area of the new P–V curve covers just 12.0615% of the original P–V curve under PSC. This area is extremely small and suggests a very good accuracy of the proposed localization scheme. The maximum area occurred at the partial shading pattern corresponding to an irradiance set of [500, 500, 600] W/m^2 for the three modules respectively. Also, the minimum area as seen in the scatter distribution covers 1.0875%, which was traced and found to occur at the partial shading pattern corresponding to [300, 200, 700] W/m^2. Averagely we see that the area distribution is concentrated around 8%. Hence the mean area of the

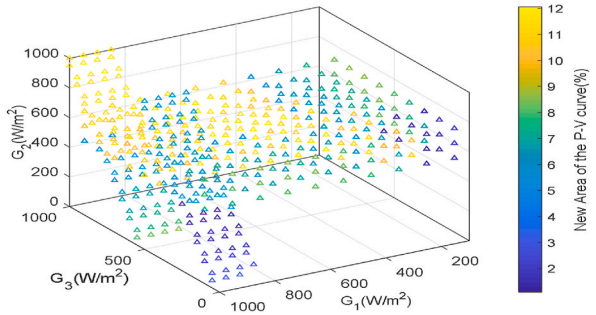

Fig. 19. Distribution of the new area of the P–V curve evaluated from the PV array using 700 PSC patterns.

new P–V curve was precisely found to be 8.262%. These important results suggest that by locating the optimal power point as proposed in this paper, we can reduce the actual P–V curve to up to 8.262%.

6. Relevance of the proposed localization scheme

Numerous MPPT algorithms fail to effectively track the maximum power point under PSC due to the lack of knowledge to distinguish between the LMPP and the GMPP or optimum power point. The conventional algorithms simply get stuck at the LMPP. So many modifications to the simple conventional algorithms have been reported in existing literature. Most of these modifications introduce a trade-off between performance and complexity. To consolidate simplicity within the context of maximum power point tracking, it is important to get back to the simple conventional algorithms such as the INC and the P&O. But the main problem is that these algorithms are specialized for single maximum power problems that are under uniform irradiance conditions.

The proposed localization scheme of the optimal power regions resulted in a conversion of the multiple power point P–V curve to a single maximum power point P–V curve under PSC. It was demonstrated that by locating the optimal power regions, we directly get rid of the local maxima. Recalling the case of the PV array under PSC-B, we see in Fig. 20, that the resulting P–V curve after locating the optimal power region does not contain a local maximum. It embeds only a single maximum power point, which is the GMPP of the PV system. By so doing, the MPPT problem is converted to a single maximum power point exercise. Hence the simple conventional MPPT algorithms whose specialty is the single MPP problem can be deployed within these regions to fast-track the global maximum power point. Furthermore, we found out that the new single MPP curve covers an average of 8.2620% of the original P–V curve under PSC. This reduced region signifies that the final maximum power point could be fast-tracked by the conventional algorithms without facing the problems of local convergence or steady-state inaccuracy.

7. Conclusion

There is a noticeable amount of power lost when PV systems are subject to partial shading conditions (PSC). Therefore, to optimize such systems, it is imperative to ensure that they operate at the global maximum power point (GMPP) irrespective of environmental constraints. This paper presented a new study aimed at providing a novel avenue for improving the performance of simple MPPT algorithms. The complex issues of multiple power points in PV systems under PSC were reduced to a single MPP task. By so doing the conventional MPPT algorithms which provide simple implementation solutions could be deployed to finalize the search for the maximum power point. The proposed system is quite simple and feasible in terms of realization. It incorporates a simple current-voltage sensor-based estimator of solar irradiance on partially shaded modules and a constructed neural network for precise determination of the optimal power areas of the PV array. We found that the optimal area of the PV system under PSC could be precisely determined under a broad spectrum of different partial shading patterns. By locating these regions, we directly reduced the MPPT problem to a single MPP task. Studies with 735 patterns of solar irradiance revealed that the new area of the PV curve was reduced to 8.2620% of its original P–V curve. This new region from an MPPT search point of view, represents an extremely reduced search space. This new study is paving the way for the improvement of maximum power point tracking under partial shading. Future works of this study will be directed toward the practical prototype and realization of the proposed system and its actual deployment in MPPT algorithms.

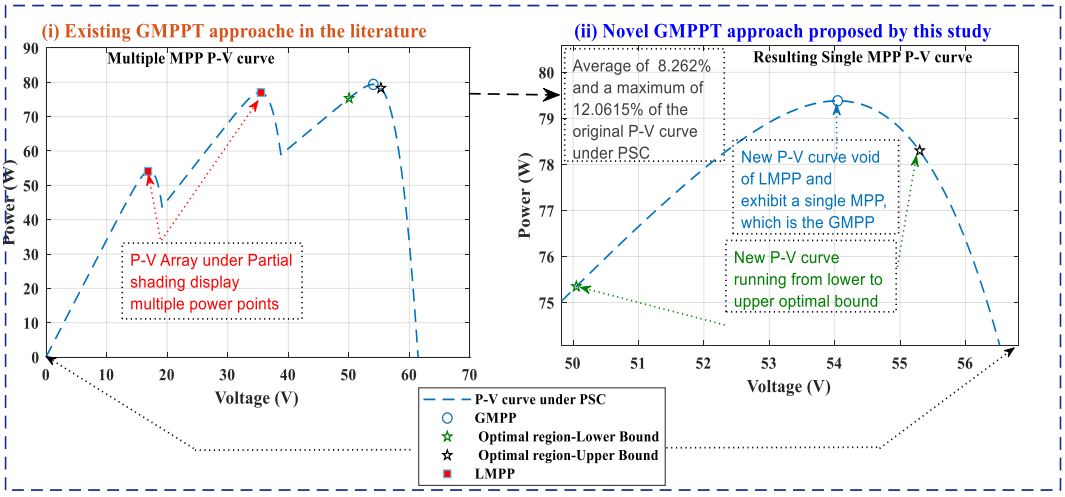

Fig. 20. Conversion of the multiple power point P–V curve to a single maximum power point P–V curve under PSC.

Author contribution statement

Ambe Harrison: Conceived and designed the experiments; performed the experiments; analyzed and interpreted the data; wrote the paper.

Njimboh Henry Alombah: performed the experiments; analyzed and interpreted the data; wrote the paper.

Jean de Dieu Nguimfack Ndongmo: Contributed reagents, materials, analysis tools and data; wrote the paper.

Data availability statement

Data will be made available on request.

Declaration of competing interest

The authors declare that they have no known competing financial interests or personal relationships that could have appeared to influence the work reported in this paper.

Appendix A

Proof of the Immersion & Invariance Estimator of solar irradiance

In the realm of immersion and invariance, to show that the estimate of solar irradiance will converge to is actual value that is $\lim_{t\to\infty}\widehat{G}(t) = G$, we have to establish that the mapping $G \longmapsto \Omega(G,.)$ has strict monotonicity feature with respect to G.

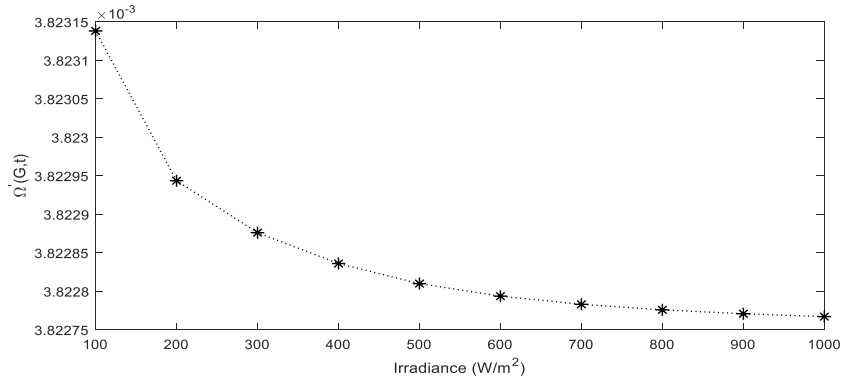

Figure. A1: Trajectory of $\frac{\partial}{\partial G}\Omega(G,t)$ for different values of irradiance

We proceed by recalling the definition of $\Omega(G,t)$, that is:

$$\Omega(G,t) = I_{ph}(G,T) - \frac{A_0}{G}\left(V_{pv} + A_1 I_{pv}\right) \tag{A1}$$

For the nonlinear differentiable regressor function $\Omega(G,t)$, strict monotonicity can be confirmed from the monotonicity of its gradient with respect to G. In different words, the function $\Omega(G,t)$ admit a monotonically increasing behavior if the following condition holds:

$$\frac{\partial}{\partial G}\Omega(G,t) > 0, \forall t > 0 \tag{A2}$$

And the function is monotonically decreasing ifIn this vein, the partial derivative of $\Omega(G,t)$ with respect to G, yields:

$$\frac{\partial}{\partial G}\Omega(G,t) = \frac{I_{ph}(G,T)}{dt} + \frac{A_0}{G^2}\left(V_{pv} + A_1 I_{pv}\right) \tag{A3}$$

But we recall that $I_{ph}(G,T)$ was defined in Eq. (2) as $I_{ph}(G,T) = \frac{G}{G_{ref}}\left(I_{ph-ref} + K_i(T - T_{ref})\right.$, with this information, Eq. (A3) can be simplified as follows:

$$\frac{\partial}{\partial x}\Omega(G,t) = \frac{1}{G_{ref}}\left(I_{ph-ref} + K_i\left(T - T_{ref}\right) + \frac{A_0}{G^2}\left(V_{pv} + A_1 I_{pv}\right)\right. \tag{A4}$$

Proposition 1. *The PV array does not operate in a faulty regime such that V_{pv}, I_{pv} are always greater than zero.*

Therefore, by inspection of the above Eq. (A4) with the satisfaction of Proposition.1, we can infer that the middle term $K_i(T - T_{ref})$ is

small as compared to the other terms, leading to the deduction that $\frac{\partial}{\partial x}\Omega(G,t) > 0$. Hence, $\Omega(G,t)$ is strictly monotonically decreasing. Fig. A1 shows $\frac{\partial}{\partial G}\Omega(G,t)$ as a function of irradiance (G). This figure verifies that $\frac{\partial}{\partial G}\Omega(G,t) < 0$.

Furthermore, the function satisfies:

$$(\widehat{G}(t) - G)[\Omega(\widehat{G}(t), t) - \Omega(G, t)] > 0, \forall \widehat{G}(t) \neq G \tag{A5}$$

The following quadratic Lyapunov candidate is put forward:

$$V(\widehat{G}) = \frac{1}{2k}(\widehat{G} - G)^2 \tag{A6}$$

Its derivative, along the trajectory of Eqs. 8–11 *is given as.*

$$\dot{V} = \frac{1}{2k}(\widehat{G}(t) - G)[\Omega(\widehat{G}, t) - \Omega(G, t)] < 0, \forall \widehat{G}(t) \neq G \tag{A7}$$

Where the bound follows immediately from Eq. (A5), *which guarantees the global asymptotic convergence of the system* (*Lyapunov second stability theorem*)

References

[1] S. Allahabadi, H. Iman-Eini, S. Farhangi, Fast artificial neural network based method for estimation of the global maximum power point in photovoltaic systems, IEEE Trans. Ind. Electron. 69 (6) (Jun. 2022) 5879–5888, https://doi.org/10.1109/TIE.2021.3094463.

[2] A. Harrison, E.M. Nfah, J. de Dieu Nguimfack Ndongmo, N.H. Alombah, An enhanced P&O MPPT algorithm for PV systems with fast dynamic and steady-state response under real irradiance and temperature conditions, Nov. 2022, Int. J. Photoenergy (2022) 1–21, https://doi.org/10.1155/2022/6009632.

[3] P.N. Tawiah-Mensah, J. Addison, S.D. Oppong, F.B. Effah, An Improved Perturb and Observe Maximum Power Point Tracking Algorithm with the Capability of Drift Avoidance in PV Systems, IEEE Xplore, Aug. 01, 2022. https://ieeexplore.ieee.org/document/9905377/. accessed Mar. 02, 2023.

[4] A. Harrison, N.H. Alombah, J. de Dieu Nguimfack Ndongmo, A new hybrid MPPT based on incremental conductance-integral backstepping controller applied to a PV system under fast-changing operating conditions, Feb. 2023, Int. J. Photoenergy (2023) 1–17, https://doi.org/10.1155/2023/9931481.

[5] N. Kumari, V.S.V. Kaumudi Pravallika, Fuzzy Based Improved Incremental Conductance MPPT Algorithm in PV System, IEEE Xplore, Jul. 01, 2020. https://ieeexplore.ieee.org/document/9198384. accessed Mar. 02, 2023.

[6] A. Harrison, J. de Dieu Nguimfack Ndongmo, N.H. Alombah, Robust nonlinear control and maximum power point tracking in PV solar energy system under real environmental conditions, Dec. 2022, ASEC (2022), https://doi.org/10.3390/asec2022-13779.

[7] F. Bayrak, G. Ertürk, H.F. Oztop, Effects of partial shading on energy and exergy efficiencies for photovoltaic panels, J. Clean. Prod. 164 (2017) 58–69, https://doi.org/10.1016/j.jclepro.2017.06.108.

[8] M.A.A. Mamun, M. Hasanuzzaman, J. Selvaraj, Experimental investigation of the effect of partial shading on photovoltaic performance, IET Renew. Power Gener. 11 (7) (May 2017) 912–921, https://doi.org/10.1049/iet-rpg.2016.0902.

[9] K.O. Sarfo, W.M. Amuna, B.N. Pouliwe, F.B. Effah, An Improved P&O MPPT Algorithm under Partial Shading Conditions, IEEE PES/IAS PowerAfrica, Aug. 2020, 2020, https://doi.org/10.1109/powerafrica49420.2020.9219851.

[10] Kok Soon Tey and S.Mekhilef, Modified incremental conductance algorithm for photovoltaic system under partial shading conditions and load variation, IEEE Trans. Ind. Electron. 61 (10) (2014) 5384–5392, https://doi.org/10.1109/tie.2014.2304921.

[11] A. Kouchaki, H. Iman-Eini, B. Asaei, A new maximum power point tracking strategy for PV arrays under uniform and non-uniform insolation conditions, Sol. Energy 91 (May 2013) 221–232, https://doi.org/10.1016/j.solener.2013.01.009.

[12] H. Patel, V. Agarwal, Maximum power point tracking scheme for PV systems operating under partially shaded conditions, IEEE Trans. Ind. Electron. 55 (4) (Apr. 2008) 1689–1698, https://doi.org/10.1109/tie.2008.917118.

[13] M. Kamran, M. Mudassar, M.R. Fazal, M.U. Asghar, M. Bilal, R. Asghar, Implementation of Improved Perturb & Observe MPPT Technique with Confined Search Space for Standalone Photovoltaic System, Journal of King Saud University - Engineering Sciences, Jun, 2018, https://doi.org/10.1016/j.jksues.2018.04.006.

[14] C.C.W. Chang, T.J. Ding, M.A.S. Bhuiyan, K.C. Chao, M. Ariannejad, H.C. Yian, Nature-inspired optimization algorithms in solving partial shading problems: a systematic review, Arch. Comput. Methods Eng. 30 (1) (Aug. 2022) 223–249, https://doi.org/10.1007/s11831-022-09803-x.

[15] L. Gao, L. Gopal, F.H. Juwono, H.-C. Ling Choo, Thomas Anung Basuki, A novel global MPPT technique using improved PS-FW algorithm for PV system under partial shading conditions, 114639, Energy Convers. Manag. 246 (Oct. 2021) 114639, https://doi.org/10.1016/j.enconman.2021.114639.

[16] L. Gong, G. Hou, C. Huang, A two-stage MPPT controller for PV system based on the improved artificial bee colony and simultaneous heat transfer search algorithm, ISA (Instrum. Soc. Am.) Trans. 132 (Jan. 2023) 428–443, https://doi.org/10.1016/j.isatra.2022.06.005.

[17] A. Harrison, Njimboh Henry Alombah, A new high-performance photovoltaic emulator suitable for simulating and validating maximum power point tracking controllers, Apr. 2023, Int. J. Photoenergy (2023) 1–21, https://doi.org/10.1155/2023/4225831.

[18] R.H.G. Tan, P.L.J. Tai, V.H. Mok, Solar irradiance estimation based on photovoltaic module short circuit current measurement, in: 2013 IEEE International Conference On Smart Instrumentation, Measurement And Applications (ICSIMA), 2013, https://doi.org/10.1109/icsima.2013.6717943.

[19] N.R. Laura, I. Delgado-Huayta, J.L. Azcue, J.C. Colque, Estimation of incident irradiance on a photovoltaic panel by the internal dynamic resistances method, in: 2020 IEEE XXVII International Conference On Electronics, Electrical Engineering And Computing (INTERCON), Sep. 2020, https://doi.org/10.1109/intercon50315.2020.9220266.

[20] C.F. Abe, J.B. Dias, G. Notton, P. Poggi, Computing solar irradiance and average temperature of photovoltaic modules from the maximum power point coordinates, IEEE J. Photovoltaics 10 (2) (Mar. 2020) 655–663, https://doi.org/10.1109/jphotov.2020.2966362.

[21] M. Carrasco, F. Mancilla-David, R. Ortega, An estimator of solar irradiance in photovoltaic arrays with guaranteed stability properties, IEEE Trans. Ind. Electron. 61 (7) (Jul. 2014) 3359–3366, https://doi.org/10.1109/TIE.2013.2281154.

[22] Xiangbin Liu, R. Ortega, Hongye Su, Jian Chu, Immersion and Invariance Adaptive Control of Nonlinearly Parameterized Nonlinear Systems," 2009, American Control Conference, 2009, https://doi.org/10.1109/acc.2009.5160204.

[23] X. Liu, R. Ortega, H. Su, J. Chu, On adaptive control of nonlinearly parameterized nonlinear systems: towards a constructive procedure, Syst. Control Lett. 60 (1) (Jan. 2011) 36–43, https://doi.org/10.1016/j.sysconle.2010.10.004.

[24] A. Industries, Adafruit INA260 High or Low Side Voltage,Current, Power Sensor. https://www.adafruit.com/product/4226 accessed Nov. 20, 2022.

[25] M. Blonquist, S. Smith, Accurate, low-cost solar irradiance measurements from a new, compact thermopile pyranometer, Accessed: Nov. 07, 2022. [Online]. Available: https://www.apogeeinstruments.com/content/apogee-SP-510-comparison-poster.pdf.